THE JOURNAL OF PHYSICAL CHEMISTRY C

Article

pubs.acs.org/JPCC

Thermodynamic and Modeling Study of Thin *n*-Heptane Films Adsorbed on Magnesium Oxide (100) Surfaces

D. Fernández-Cañoto[†,‡] and J. Z. Larese*[,†]

[†]Department of Chemistry, University of Tennessee, Knoxville, TN 37996, United States

ABSTRACT: Thermodynamic properties of *n*-heptane adsorbed on the MgO(100) surface were investigated using high-resolution, volumetric adsorption isotherms in the temperature range of 205−275 K. Two distinct molecular layers were observed in all isotherms. The heat, differential enthalpy, differential entropy, and isosteric heat of adsorption were determined. Using the temperature dependence of the two-dimensional compressibility, two phase transitions were observed at 246.0 ± 2.0 K and 249.3 ± 1.2 K for the first and second layers, respectively. The average area per *n*-heptane molecule adsorbed on MgO was estimated to be 99 ± 10 Å^2, suggesting that the carbon backbone is preferentially oriented parallel to the surface. The COMPASS force field was used to calculate the minimum energy configurations of an *n*-heptane molecule on the MgO(100) surface. The calculations support experimental evidence of the carbon backbone oriented parallel to the surface and additionally suggest a preferential alignment of the molecule along the ⟨11⟩ and ⟨10⟩ directions in the surface (100) plane.

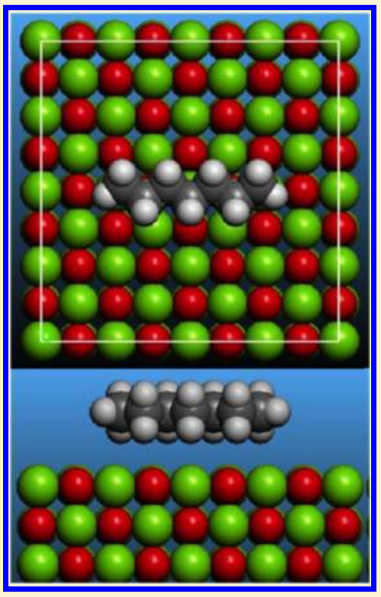

INTRODUCTION

Nanometer scale metal oxides (MOs) currently play a prominent role in materials research, especially as energy-related materials. Magnesium oxide is a prototypical MO because it is a simple ionic crystal with a rock salt structure; the Mg and O atoms form interpenetrating cubic lattices. MgO can be produced in molar quantities as nanocubes (with dimensions ≈5−50 nm) with a narrow size distribution, single facet (100) exposure, and high chemical purity, which are physical properties that make MgO well suited to basic surface science research.[1] Understanding the adsorption of molecules on solid surfaces is also central to many scientific and technological challenges such as lubrication, corrosion, heterogeneous catalysis, and adhesion. This study details the properties of the *n*-heptane MgO system with a particular focus on thermodynamics using volumetric adsorption and on structure using molecular modeling; both are in preparation for neutron investigations of microscopic structure and dynamics. In addition to being of fundamental interest, heptane adsorption studies have practical applications. For example, the isomerization of *n*-heptane over Pt-loaded beta zeolites is technologically relevant for octane enhancement processes.[2−4] Lower molecular weight and unbranched alkanes such as *n*-heptane in gasoline internal combustion engines cause engine knock, which is in contrast to other branched-chain alkane isomers which burn more slowly and thereby result in better fuel efficiency. Thus, increasing the basic information available for *n*-heptane interaction with MOs would aid in the development of hydrogenation catalysts used to enhance the isomerization of *n*-heptane into branched products.

The adsorption properties of *n*-heptane on several materials have been investigated using different techniques such as neutron scattering,[5,6] calorimetry,[7] Fourier transform infrared spectroscopy,[8] X-ray diffraction,[9] and molecular dynamics simulations.[10−12] In this study, more than 60 high-resolution volumetric isotherms, ranging in temperature from 205 to 275 K, were measured and used to calculate the area per molecule (APM) and thermodynamic properties, for example, heat and isosteric heat, differential enthalpy, and differential entropy of adsorption during the layer growth process. Furthermore, the two-dimensional isothermal compressibility was used to identify the location of possible phase transitions.

Taken in combination with our previous studies of other alkanes,[13−19] this investigation is aimed at developing a better understanding of how the phase and layering transitions and surface binding energies vary with the alkane chain length. The main purpose of these investigations is to understand how the relative strength of the molecule−substrate versus molecule−molecule interaction influences the structure and dynamics of these molecular films. Furthermore, we expect to establish

Received: July 31, 2013
Revised: January 14, 2014
Published: January 15, 2014

dx.doi.org/10.1021/jp407651t | *J. Phys. Chem. C* 2014, 118, 3451−3458

whether a systematic variation in the adsorption properties on MgO can be associated with the odd versus even members of the *n*-alkanes series. Such an effect is observed in the bulk linear alkanes as an alternation of the melting points, beginning with pentane. Odd-numbered *n*-alkanes have lower bulk melting points because they form slightly higher energy crystallites because of their inability to align themselves without creating voids.[20]

To gain additional insight into the microscopic details of the adsorption process, we performed molecular modeling using central force fields in tandem with the thermodynamic experiments. Force field methods have been used elsewhere for studying the minimum energy configuration of condensed-phase systems.[21−23] The condensed-phase optimized molecular potentials for atomistic simulation studies[24] (COMPASS) is one such force field that has been used to explore the microscopic properties, to optimize the geometry of molecular adsorbates, and to connect the microscopic behavior to thermodynamic (macroscopic) quantities determined from experimental investigations. More specifically, good agreement with experiment has been realized using COMPASS to calculate the heat of adsorption of several molecules adsorbed on MgO.[25,26] In the work described below, we use the COMPASS force field to determine minimum energy configurations of the physisorbed state of *n*-heptane on MgO. Our long-term objective is to aid in the development of accurate and reliable interaction potentials for describing the physical properties of molecular adsorption on MgO surfaces.

EXPERIMENTAL SECTION

The MgO powders used in this study were produced using a patented method developed by Kunnman and Larese[27] and are composed of nanocubes with a narrow particle size distribution (typically 250 ± 30 nm) as determined by transmission electron microscopy (TEM) based particle size analysis. The MgO has an average surface area of ≈8 $m^2\ g^{-1}$ and exhibits essentially single facet exposure of the (100) face.[13] Before use, the MgO powder was heat-treated in vacuo (<10^{-7} Torr) at 950 °C for >36 h.

Several different aliquots of the same MgO batch were used during the course of this study. Samples (≈0.4 g) were loaded inside an oxygen-free high conductivity copper cell sealed with an indium gasket in an argon-filled glovebox to prevent surface contamination and hydroxylation from the atmosphere. The filled cell was then mounted on a closed-cycle helium refrigerator (APD Cryogenics), and adsorption isotherms were measured volumetrically using an in-house built, automated apparatus.[28] A Neocera Model 21 temperature controller and a platinum thermometer were used to regulate the temperature within 2 mK. The *n*-heptane (>99% anhydrous, Acros Organics) was further purified using sodium metal as a drying agent and multiple freeze−pump−thaw cycles using a liquid nitrogen bath and a turbomolecular pump based vacuum system (<10^{-7} Torr). When the total quantity of gas added to the cell was greater than 20 nominal layers, the equilibrium pressure, p_f, was found to be quasi-constant and was deemed to correspond to the saturated vapor pressure (SVP = p_0) of bulk *n*-heptane. The sample temperatures were determined using the semiempirical Antoine equation

$$T\ [\mathrm{K}] = \frac{b}{a - \log(P[\mathrm{bar}])} - c$$

with coefficients a = 4.81803, b = 1635.409, and c = −27.338.[29] It was necessary to perform a dead-space correction to account for the *n*-heptane molecules that occupy the gas phase in the sample cell.

RESULTS AND DISCUSSION

Thermodynamic Measurements. Volumetric isotherms are used in this study to identify the monolayer capacity for *n*-heptane as compared to methane on MgO (see Figure 1). The

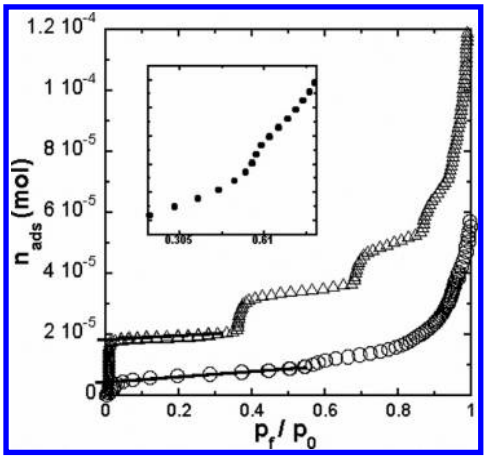

Figure 1. A methane isotherm (Δ) at 73.8 K was performed to calculate the specific surface area of the MgO sample (≈8 $m^2\ g^{-1}$) and to verify sample quality. A volumetric isotherm of *n*-heptane at 217.9 K (○) shows the second layer, detailed in the inset. Lines are drawn to identify the point used to calculate areas per molecule. Surface molar capacity for *n*-heptane is approximately 5.5 times lower than the capacity for methane on MgO.

surface area per molecule of *n*-heptane (APM) is found to be 99 ± 10 Å^2. Comparison of the APM of *n*-heptane to previous alkane isotherm studies on MgO[13−19] suggests that the *n*-heptane molecules also adsorb with their carbon backbone parallel to the surface.

Isotherms were recorded between the temperatures of 205 K (SVP = 0.308 Torr) and 275 K (SVP = 12.3 Torr), a range bounded above by the requirement that the sample be colder than ambient temperature and bounded below by the sensitivity of the pressure measurement device in the range of the monolayer riser.

Figure 2 displays a subset of five isotherms between 244.2 and 252.2 K. As noted above, two adsorption steps were observed for all of the isotherms recorded in this study; the second step is more prominent at lower temperature. Thermodynamic properties of the system are assigned by the locations of each adsorption step. As described previously,[13−19] the position of each adsorption step can be accurately located by using the numerical first derivatives $\Delta n_{ads}/\Delta p_f$ [mol·torr^{-1}].

Figure 3 shows a representative isotherm of *n*-heptane on MgO recorded at 217.9 K along with the numerical first derivative. The equilibrium pressure of the monolayer step at the various temperatures is analyzed using the Clausius−Clapeyron (C−C) method $\ln(p_f^i) = A^i/T + B^i$ where p_f^i [torr] is the location of the i adsorption step; i = [1, 2, ∞ ⇒ SVP].

Figure 4 displays the (C−C) fit to the data. The differential enthalpy (ΔH^i), entropy (ΔS^i), and heat of adsorption (Q_{ads}^i) can then be calculated using the following relations:

$$\Delta H^i = -R\cdot(A^i - A^\infty) \quad (1)$$

dx.doi.org/10.1021/jp407651t | J. Phys. Chem. C 2014, 118, 3451−3458

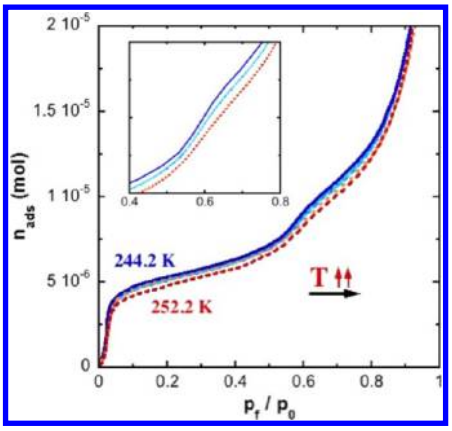

Figure 2. A set of five isotherms between 244.2 K (solid blue line) and 252.2 K (dashed red line) with intermediate temperatures 246.3, 248.2, and 250.1 K are shown. The number of moles adsorbed is plotted as a function of the reduced pressure, p_f/p_0 (i.e., the ratio of the equilibrated pressure and the SVP). Notice that as the temperature approaches 250 K the second step is much less pronounced indicating the possibility that a phase transition takes place. The dotted lines represent the isotherms at 246.3 and 248.2 K, and the dashed-dotted line represents the isotherm at 250.1 K. This change in the preeminence of the second step region is more apparent in the inset.

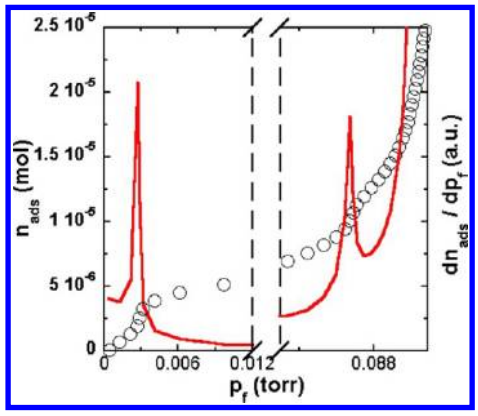

Figure 3. Heptane isotherm at 217.9 K (○) is plotted with its corresponding numerical derivative (solid line). The maximum of the peaks represents the equilibrium pressure (p_f^i) of layer formation.

$$\Delta S^i = -R\cdot(B^i - B^\infty) \tag{2}$$

$$Q_{ads}^{\ i} = R\cdot A^i \tag{3}$$

Thermodynamic quantities calculated using eqs 1−3 are given in Table 1 along with the C−C coefficients.

The values of Q_{ads}, ΔH, and ΔS can be interpreted by comparing the behavior of the layered phase and the bulk phase. Because the isotherms were recorded between the triple point (182.56 K) and the critical point (540 K), the thermodynamic values of the adsorbed film should be compared to the vaporization phase transition, $\Delta H_{vap} \approx 38$ kJ·mol^{-1} at 275 K and $\Delta H_{vap} \approx 42$ kJ·mol^{-1} at 205 K.[30,31] The C−C analysis indicates that Q_{ads} approaches the expected values. The trends observed for ΔH and ΔS both in sign and in magnitude show that monolayer adsorption is favored entropically as well as energetically compared to bulk. Thermodynamically, the second layer behaves more like bulk heptane than the first. This clearly indicates that molecule−molecule (M−M) interaction in the second layer is more dominant than

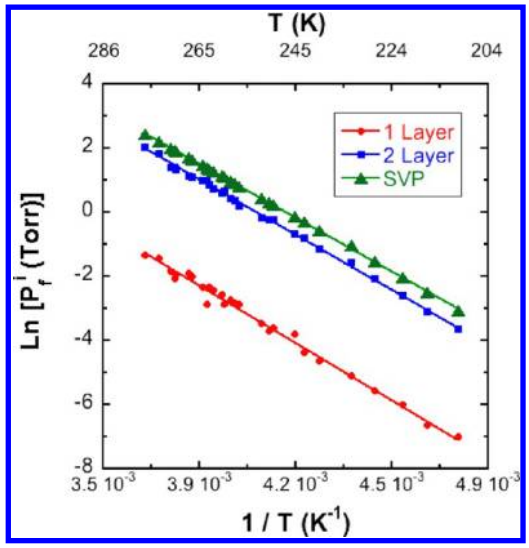

Figure 4. Clausius−Clapeyron fit on the equilibrium pressure steps p_f^i from the two layers (●, i = 1; ■, i = 2) and for SVP (▲) values. From the linear fit parameters, the heats of adsorption, differential enthalpy, and entropy are calculated.

molecule−substrate (M−S) interactions in contrast to the first layer which is more strongly influenced by its proximity to the MgO surface. At a given coverage (isostere, fixed ϑ), the heat of vaporization can be determined using the following simplifying assumption:[32]

$$Q_{st} = R\bar{T}^2\left(\frac{\partial \ln(p_f)}{\partial T}\right)_\vartheta \cong R\bar{T}^2\left(\frac{\Delta \ln(p_f)}{\Delta T}\right)_\vartheta \tag{4}$$

Figure 5 was produced using eq 4 and isotherms at 210.2 and 212.2 K. The figure clearly shows that monolayer and bilayer adsorption is energetically favorable. As the film thickness increases beyond second layer completion, Q_{st} approaches 34.0 kJ·mol^{-1}, a value that compares favorably with the heat of vaporization of bulk heptane (31.5 ± 1.6 kJ·mol^{-1})[30,31] at the highest coverages examined.

As is observed in bulk materials, a change in compressibility (K) can be used to identify a phase boundary.[19] At equilibrium, the chemical potential difference between a two-dimensional (2D) film and its coexisting three-dimensional (3D) vapor is zero. Analogous to 3D, the 2D isothermal compressibility for an adsorbed film can be determined using the following:

$$K_{2D} = \frac{A\cdot p_f}{N_A\cdot k_B\cdot T\cdot n_{ads}^2}\cdot\frac{\Delta n_{ads}}{\Delta p_f} \tag{5}$$

where A is the surface area of the sample in m^2, T is the temperature in K, N_A is Avogadro's number, n_{ads} is the number of molecules adsorbed, and k_B is Boltzmann's constant.[33]

Figure 6 contains a representative set of K_{2D} calculated at several temperatures using eq 5. At lower temperatures, K_{2D} is characterized by sharp narrow peaks that are nearly temperature independent. However, as shown in Figure 7, the K_{2D} peaks steadily decrease in height and broaden as the temperature rises.

Using the temperature dependence of the width of K_{2D} as a guide above ≈245 K, two possible phase transitions can be located at 246.0 ± 2.0 K and 249.3 ± 1.2 K for the first and second layers, respectively. Because it is well established that melting of monolayer solids occurs around 70% of the bulk

dx.doi.org/10.1021/jp407651t | J. Phys. Chem. C 2014, 118, 3451−3458

Table 1. Thermodynamic Parameters Calculated from Clausius−Clapeyron Equation for *n*-Heptane Adsorbed on MgO

layer	A [K]	B	Q [kJ·mol^{-1}]	ΔH [kJ·mol^{-1}]	ΔS [J·mol^{-1}K^{-1}]
1	−5097 ± 97.8	17.34 ± 0.40	42.38 ± 1.00	−2.55 ± 0.02	21.73 ± 0.50
2	−4880.2 ± 45.3	19.80 ± 0.18	40.58 ± 0.50	−0.74 ± 0.01	1.31 ± 0.20
SVP	−4791.3 ± 15.8	19.95 ± 0.06	39.84 ± 0.20		

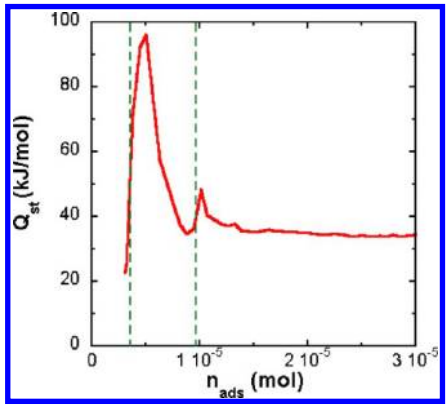

Figure 5. Isosteric heat of adsorption Q_{st} versus coverage at 211.2 K. The temperature interval used in this calculation is ΔT ± 2 K. Monolayer coverage is completed at ±3.75 × 10^{-6} moles, and the second layer is completed at ≈9.4 × 10^{-6} moles as indicated by the dashed lines.

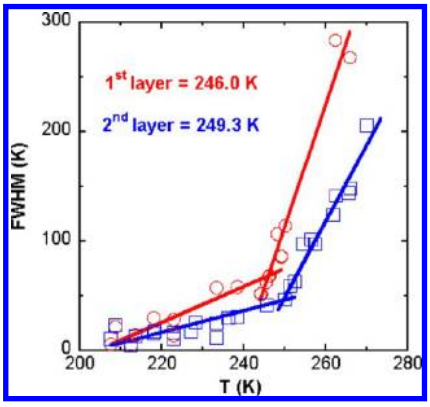

Figure 7. Full-width at half maximum of K_{2D} for the first (○) and second (□) layers versus temperature. Locations of possible phase transitions of the first and second layers occur at 246.0 ± 2.0 K and at 249.3 ± 1.2 K, respectively.

melting point, we suggest that the identified transition represents a 2D liquidlike (L) to a hypercritical fluid (F) phase transition. Previous neutron scattering measurements have shown that a monolayer *n*-hexane film on MgO melts at ≈30 K below the triple point (T_{triple} = 178 K), a somewhat higher temperature than the expected 0.7 times the bulk melting temperature. All of the isotherms reported here for *n*-heptane are measured above the triple point; the proposed L → F transition occurs well below T_c, the bulk critical point. The transition temperature of the monolayer film is a resultant of stronger M−S interaction, whereas the second layer is spatially removed from the MgO surface causing the second-layer phase-transition temperature to be closer to the bulk transition.

Molecular Simulation. These calculations were performed using the Forcite geometry optimization algorithm in Materials Studio, a program suite available from Accelrys Software Inc. This algorithm is an iterative calculation that proceeds until the total energy of a molecular structure is minimized. The calculated total energy is equal to the total enthalpy at zero Kelvin but neglects quantum effects (i.e., zero point motion). As noted earlier, the COMPASS force field was used for these geometry optimizations of an *n*-heptane molecule on the MgO surface. The functional form for the total energy used in this particular force field can be divided into two portions: one that deals with the valence terms and the other that addresses the nonbonded interaction terms. Our interest here is to focus on the nonbonded energies, E_{nb}, which represent most of the energetic contributions to the binding energy of a physisorbed molecule. The functional form for the nonbonded contributions includes a Lennard-Jones (L-J) term and a Coulombic term which account for the van der Waals and the electrostatic

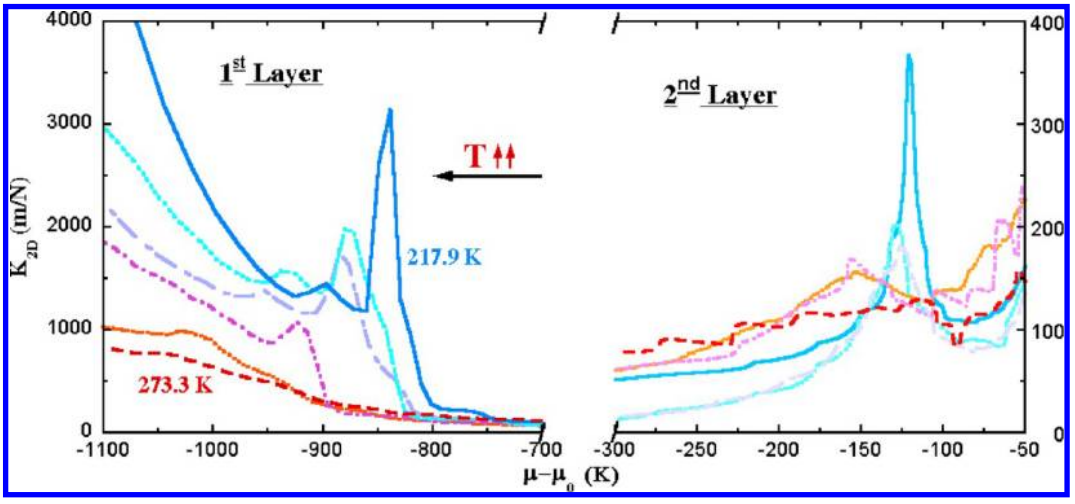

Figure 6. Representative plots of the isothermal compressibility for the first and second layers as a function of the chemical potential difference of the chemical potential of the film, μ, and the chemical potential of the bulk phase, μ_0, given by k_BT ln p_f or k_BT ln p_0, respectively, for a temperature range of 217.9 K (solid line) to 273.9 K (dashed line).

dx.doi.org/10.1021/jp407651t | J. Phys. Chem. C 2014, 118, 3451−3458

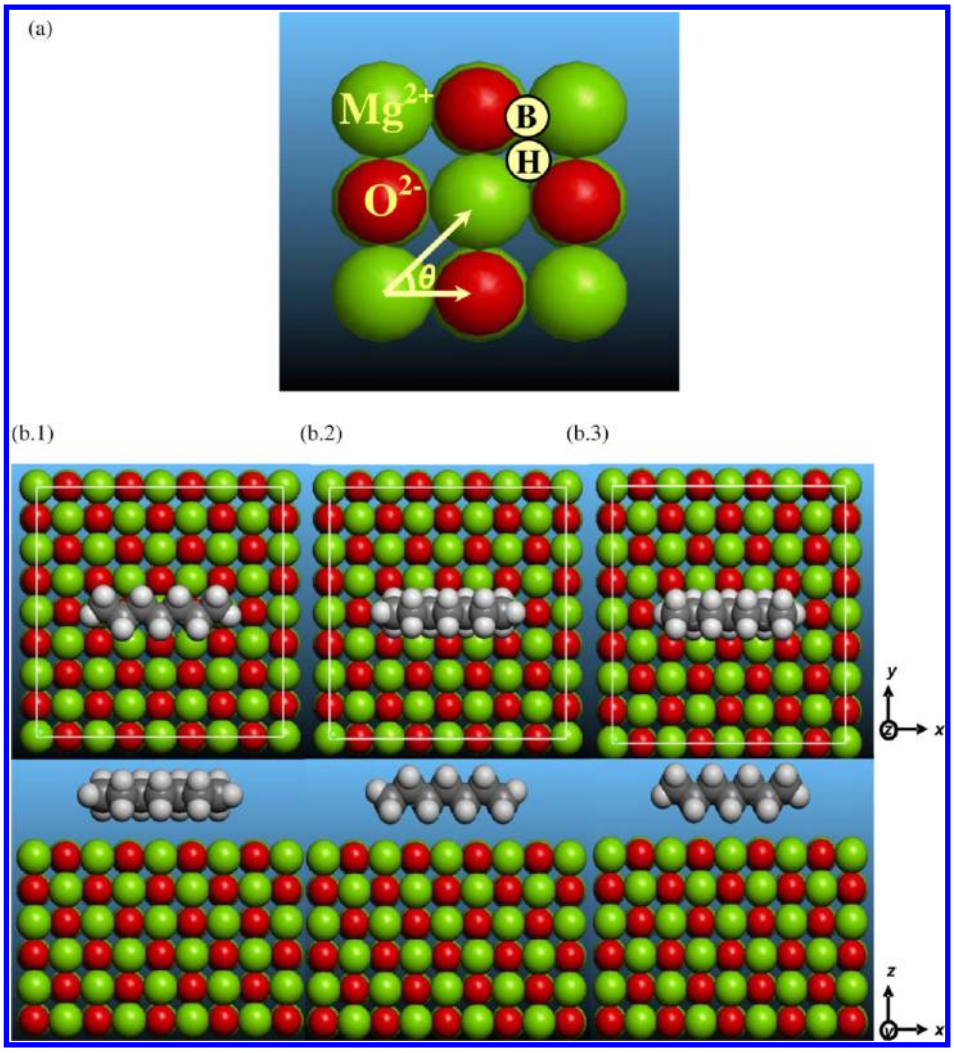

Figure 8. (a) Principal adsorption sites on the MgO(100) surface: atop of Mg^{2+}, O^{2-}, bridge (B), and hollow (H). (b) Simulations started with the *n*-heptane center of mass placed at the principal adsorption sites. Here, they are illustrated for the three initial configurations CC7 (b.1), CC4 (b.2), and CC3 (b.3) for *n*-heptane molecules placed atop of the Mg^{2+} and rotated $\theta = 0°$ to the *x*-axis.

interactions, respectively. Further details about the functional form of the COMPASS force field can be found elsewhere.[24]

The energy optimization was performed using the Forcite Smart algorithm, which is a standard cascade of steepest descent,[34] ABNR[35] (adjusted basis set Newton−Raphson), and quasi-Newton methods,[36] to improve the efficiency of the calculations. The convergence criterion was set at a maximum of 5000 iterations with the optimization thresholds for the energy, force, and displacement set at 2×10^{-5} kcal·mol^{-1}, 1×10^{-3} kcal·Å^{-1}, and 1×10^{-6} Å, respectively. The nonbonded energies were computed via Ewald summation.[37] The lattice parameters of the MgO slab used were $a = b = 16.8448$ Å and $c = 10.5280$ Å. The MgO substrate slab and an individual *n*-heptane molecule were first optimized separately, and the lattice parameters of the slab were then constrained to the optimized values for the rest of the investigation.

Energy optimizations performed with initial configurations of the carbon−carbon axis perpendicular to the surface plane always resulted in final configurations with the CC axis parallel to the surface. Therefore, we concentrated on three different initial CC orientations of the molecule. The first has the molecular plane containing the CC backbone parallel to the MgO(100) surface with all seven carbon atoms equidistant from the surface. The other two have the plane containing the carbon backbone perpendicular to the MgO(100) surface: one with four carbon atoms equidistant and closest to the surface and the other with three carbons equidistant and closest to the surface. We refer to these three different orientations as CC7, CC4, and CC3, respectively. To limit the scope of this study, we restricted our optimization studies to molecular configurations near adsorption sites of high symmetry. Four such sites were used in the initial placement of the *n*-heptane molecule: atop a Mg atom, atop an O atom, in the hollow (H) vacancy between four surface atoms, or in the bridge (B) vacancy between two surface atoms (see Figure 8 b). The center of mass (COM) of a single heptane molecule was placed at one of these sites with the molecule in one of the three CC configurations and the CC backbone pointing in the ⟨10⟩ direction. Next, the Forcite algorithm was used to minimize the energy, and the resulting molecular conformation and energy were recorded. This energy minimization process is repeated at each adsorption site by returning the COM of the molecule to its initial position and then by sequentially rotating the molecule through the angle θ about an axis perpendicular to the surface plane (Figure 8 a). Ten different equal steps of θ over an angular range of 45° were examined, thereby sampling

dx.doi.org/10.1021/jp407651t | J. Phys. Chem. C 2014, 118, 3451−3458

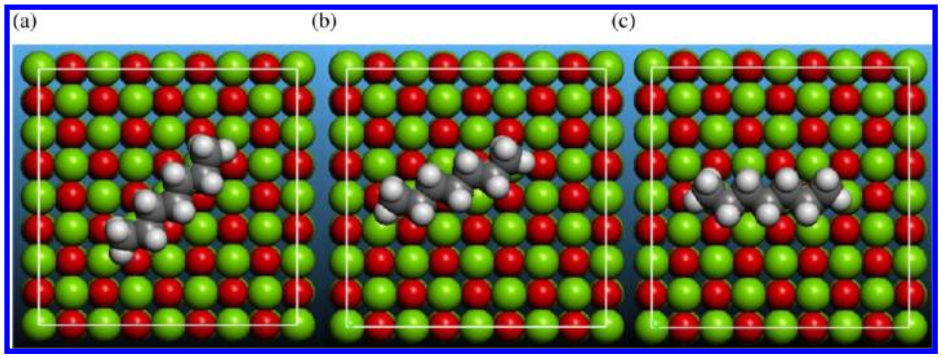

Figure 9. *n*-Heptane geometry optimizations for the CC7 structure. A single *n*-heptane molecule with its center of mass located (a) atop of the Mg^{2+} site, rotated 45° to the (100) plane, and E_{nbCCN} = −68.42 kJ·mol^{-1}; (b) above the H site, 20°, and E_{nbCCN} = −65.94 kJ·mol^{-1}; and (c) above the B site, 0°, and E_{nbCCN} = −64.49 kJ·mol^{-1}.

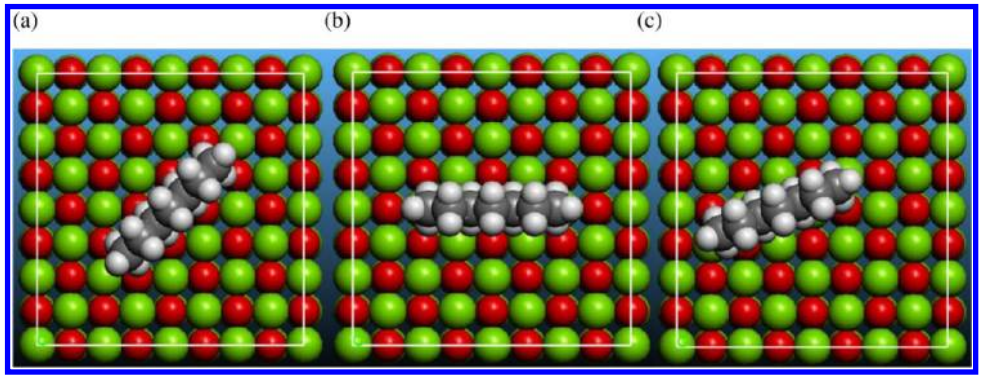

Figure 10. *n*-Heptane geometry optimizations for the CC4 structure. A single *n*-heptane molecule with its center of mass located (a) atop of the Mg^{2+} site, rotated 45° to the (100) plane, and E_{nbCCN} = −63.64 kJ·mol^{-1}; (b) above the Mg^{2+} site, 0°, and E_{nbCCN} = −59.25 kJ·mol^{-1}; and (c) above the O^{2-} site, 20°, and E_{nbCCN} = −57.94 kJ·mol^{-1}.

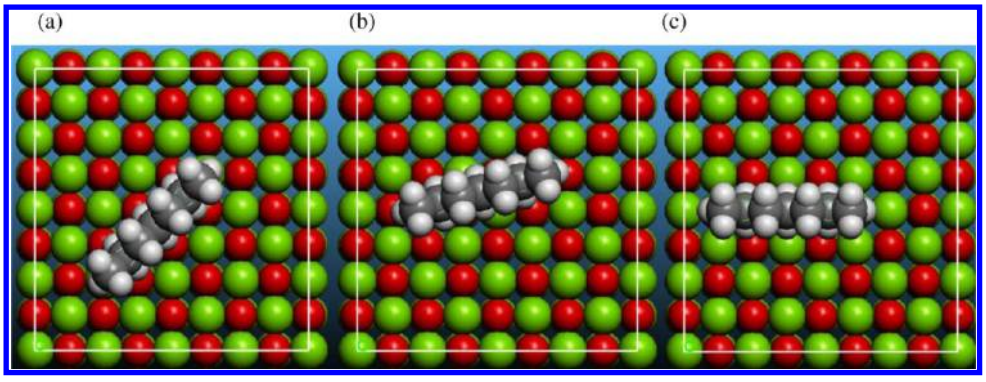

Figure 11. *n*-Heptane geometry optimizations for the CC3 structure. A single *n*-heptane molecule with its center of mass located (a) above the H site, rotated 45° to the (100) plane, and E_{nbCCI} = −57.01 kJ·mol^{-1}; (b) above the H site, 14°, and E_{nbCCI} = −55.45 kJ·mol^{-1}; and, (c) above the O^{2-} site, 0°, and E_{nbCCI} = −52.59 kJ·mol^{-1}.

the entire 4-fold MgO(100) surface symmetry. This was performed for each of the three CC backbone orientations at each of the four sites for a total of 120 initial configurations.

We will refer to the final optimized orientations of this exercise using the three identifying characteristics in the following notation: (final adsorption site of COM, final CC backbone orientation, optimized value of θ). For example, the most common final configurations of the heptane molecule occurred with the molecular axis lying along the ⟨11⟩ direction in the (100) plane and the COM located either atop the Mg^{2+} center with CC7 or CC4 orientations or at the hollow site in a CC3 orientation. These final configurations are denoted (Mg^{2+}, CC7, 45°), (Mg^{2+}, CC4, 45°), and (H, CC3, 45°), respectively. Seven other optimized molecular configurations, although statistically less likely, occurred frequently enough to warrant mentioning: (H, CC7, 20°); (H, CC3, 14°); (B, CC7, 0°); (Mg^{2+}, CC4, 0°); (O^{2-}, CC4, 20°); and (Mg^{2+}/O^{2-}, CC3, 0°). Each of these is shown in Figures 9, 10, and 11 which, along with Figure 8, were generated in Materials Studio. For each initial CC backbone configurations, Table 2 summarizes the nonbonded energy and distance from COM to the site for each of the three most probable final configurations. The percentage of calculations that resulted in these most probable configurations is also given. Several trials with the initial orientation of the CC backbone pointing perpendicular to the (100) surface plane resulted in a final configuration of the

dx.doi.org/10.1021/jp407651t | J. Phys. Chem. C 2014, 118, 3451−3458

Table 2. COMPASS Minimum Energy Configuration Results for *n*-Heptane Adsorbed on MgO

orientation	ads site	final θ	% of optimized orientations	COM to site [Å]	E_{nb} [kJ·mol^{-1}]
CC7	Mg^{2+}	45	45	3.213	−68.42
	H	20	25	3.218	−65.94
	B	0	17.5	3.223	−64.49
CC4	Mg^{2+}	45	35	3.432	−63.64
	Mg^{2+}	0	22.5	3.420	−59.25
	O^{2-}	20	17.5	3.449	−57.94
CC3	H	45	47.5	3.213	−57.01
	H	14	32.5	3.483	−55.45
	Mg^{2+}/O^{2-}	0	10	3.528	−52.59

molecule in one of the CC7, CC4, or CC3 orientations, thereby reinforcing the conjecture that the molecules are adsorbed in a parallel configuration. These results are conceptually useful because they suggest that a combination of these configurations may occur as molecules are adsorbed from the gas phase.

While the results presented here are for an isolated molecule (where molecule−molecule interactions are neglected), it is encouraging that the energy E_{nb} is about the same magnitude as the heats of adsorption determined in the thermodynamic results presented above. Because these calculations compute the enthalpy at zero Kelvin, the bulk heat of vaporization at zero Kelvin should provide a more apt comparison. On the basis of data taken from 298−363 K,[30,31] ΔH_{vap} can be extrapolated to a low temperature limit of 53.66 kJ·mol^{-1}, which compares favorably to the E_{nb} energies in Table 2. For isolated *n*-heptane molecules on the MgO(100) surface, those with the CC7 configuration have the highest binding energies, while the CC3 orientations have the lowest. Our calculations show that both the statistically most probable locations and the highest binding energies are associated with *n*-heptane orientations that minimize the distance to the MgO(100) surface for the largest number of atoms within the molecule. This is not surprising as these orientations would be expected to maximize the attractive electrostatic interactions between the molecule and the surface.

CONCLUSION

Volumetric isotherm studies of *n*-heptane adsorbed on MgO(100) between 205 and 275 K have been performed, and the adsorption thermodynamics have been quantified. Evidence for the formation of a discrete second adsorption layer is recorded within the temperature range studied. The area per molecule of *n*-heptane adsorbed on the MgO surface was estimated to be 99 Å^2, suggesting that the *n*-heptane molecules adsorb primarily with their CC backbone parallel to the surface. The isotherms were used to determine the heat, enthalpy, and entropy of adsorption for each of the two observed layers, whereby a noticeable decrease in the molecule−substrate interactions was observed when the number of surface layers was increased from one to two. Beyond two statistical layers, the wetting behavior is not layer-by-layer but appears to exhibit incomplete wetting characteristics.

Tracking the thermal evolution in peak width of the two-dimensional compressibility allows for identification of two possible phase transitions at 246.0 and 249.3 K for the first and second layer, respectively. By using the COMPASS force fields and the Forcite energy minimization algorithm, we provide additional support to the thermodynamic APM result which suggest that heptane lies with its molecular axis parallel to the (100) surface plane. Further analysis of the modeling indicates that isolated molecules most likely adsorb in the CC7 and CC4 configurations with the COM located at the Mg-atop site and aligned along the ⟨11⟩ and ⟨10⟩ direction in the MgO(100) surface. There is limited evidence for adsorption in the CC3 configuration where adsorption is above the H site. The nonbonded energies for a single molecule determined in the modeling studies are of the same order as the heat of adsorption in the monolayer regime determined in the thermodynamic experiments. No modeling evidence for perpendicular orientation of an adsorbed heptane molecule was obtained. Neutron scattering experiments are planned to investigate the structure and dynamics of the adsorbed heptane films as well as the nature and existence of the potential phase transitions identified here.

AUTHOR INFORMATION

Corresponding Author

*E-mail: jzl@utk.edu.

Present Address

‡ESS-Bilbao Edificio Cosimet. 48940 Leioa, Spain.

Notes

The authors declare no competing financial interest.

ACKNOWLEDGMENTS

The authors thank previous and current Larese group members for useful discussions and assistance, especially S. Adak, T. Arnold, N. Bass, A. Hicks, and G. Rouvelas. Special thanks to Michael Blanchard for help in *n*-heptane purification. This work was supported in part by the U.S. Department of Energy, Materials Science Division, under contract No. DE-AC05-00OR22725 with Oak Ridge National Laboratory, managed and operated by UT-Battelle, LLC.

REFERENCES

(1) Spoto, G.; Gribov, E.; Ricchiardi, G.; Damin, A.; Scarano, D.; Bordiga, S.; Lamberti, C.; Zecchina, A. Carbon Monoxide MgO from Dispersed Solids to Single Crystals: A Review and New Advances. *Prog. Surf. Sci.* **2004**, *76*, 71−146.

(2) Abudawood, R. H.; Alotaibi, F. M.; Garforth, A. A. Hydroisomerization of n-Heptane over Pt-Loaded USY Zeolites. Effect of Steaming, Dealumination, and the Resulting Structure on Catalytic Properties. *Ind. Eng. Chem. Res.* **2011**, *50*, 9918−9924.

(3) Kondo, J. N.; Yang, S.; Zhu, Q.; Inagaki, S.; Domen, K. In Situ Infrared Study of n-Heptane Isomerization over Pt/H-Beta Zeolites. *J. Catal.* **2007**, *248*, 53−59.

(4) Gopal, S.; Smirniotis, P. G. Factors Affecting Isomer Yield for n-Heptane Hydroisomerization over As-Synthesized and Dealuminated Zeolite Catalysts Loaded with Platinum. *J. Catal.* **2004**, *225*, 278−287.

(5) Castro, M.; Clarke, S.; Inaba, A.; Arnold, T.; Thomas, R. Solid Monolayers of Heptane Adsorbed to Graphite from Its Liquid. *J. Phys. Chem. Solids* **1999**, *60*, 1495−1497.

(6) Castro, M. A.; Clarke, S. M.; Inaba, A.; Thomas, R. K. Solid Monolayers Adsorbed at the (Solid-Liquid) Interface Studied by Incoherent Elastic Neutron Scattering. *J. Phys. Chem. B* **1997**, *101*, 8878−8882.

(7) Clarke, S. M.; Inaba, A.; Arnold, T.; Thomas, R. K. Calorimetric Investigation of the Monolayers Formed At Solid-Liquid Interface. *J. Therm. Anal. Calorim.* **1999**, *57*, 643−651.

(8) Oh, E.; Wurster, D. E.; Majuru, S.; Wang, J. C. T. Use of Fourier Transform Infrared (FTIR) Spectroscopy to Follow the Adsorption of

Heptane and 1,4-Dioxane Vapors on a Zinc Oxide Surface. *J. Pharm. Sci.* **1998**, *87*, 1124−1129.
(9) Arnold, T.; Dong, C. C.; Thomas, R. K.; Castro, M. A.; Perdigon, A.; Clarke, S. M.; Inaba, A. The Crystalline Structures of the Odd Alkanes Pentane, Heptane, Nonane, Undecane, Tridecane and Pentadecane Monolayers Adsorbed on Graphite at Submonolayer Coverages and from the Liquid. *Phys. Chem. Chem. Phys.* **2002**, *4*, 3430−3435.
(10) Krishnan, M.; Balasubramanian, S. Phase Behaviour of Ultrathin Crystalline n-Heptane Films on Graphite: An Atomistic Simulation Study. *Phys. Chem. Chem. Phys.* **2005**, *7*, 2044−2052.
(11) Manos, G.; Dunne, L. J.; Chaplin, M. F.; Du, Z. Comparative Study of Monte Carlo Simulations and Exact Statistical Mechanical Lattice Model of Commensurate Transitions of Alkanes Adsorbed in Zeolites. *Chem. Phys. Lett.* **2001**, *335*, 77−84.
(12) Pint, C. L. Different Melting Behavior in Pentane and Heptane Monolayers on Graphite: Molecular Dynamics Simulations. *Phys. Rev. B* **2006**, *73*, 045415.
(13) Freitag, A.; Larese, J. Z. Layer Growth of Methane on MgO: An Adsorption Isotherm Study. *Phys. Rev. B* **2000**, *62*, 8360.
(14) Arnold, T.; Cook, R. E.; Larese, J. Z. Thermodynamic Investigation of Thin Films of Ethane Adsorbed on Magnesium Oxide. *J. Phys. Chem. B* **2005**, *109*, 8799−8805.
(15) Felty, M. Ph.D. Thesis, University of Tennessee, Knoxville, TN, 2008.
(16) Arnold, T.; Chanaa, S.; Clarke, S. M.; Cook, R. E.; Larese, J. Z. Structure of an n-Butane Monolayer Adsorbed on Magnesium Oxide (100). *Phys. Rev. B* **2006**, *74*, 085421.
(17) Cook, R. Ph.D. Thesis, University of Tennessee, Knoxville, TN, 2006.
(18) Yaron, P. N.; Telling, M. T. F.; Larese, J. Z. Thermodynamic Investigation of n-Hexane Thin Films Adsorbed on Magnesium Oxide. *Langmuir* **2006**, *22*, 7203−7207.
(19) Sprung, M.; Larese, J. Z. Adsorption Isotherm Studies of Methyl Chloride on MgO. *Phys. Rev. B* **2000**, *61*, 13155−13158.
(20) Boese, R.; Weiss, H.-C.; Bläser, D. The Melting Point Alternation in the Short-Chain *n*-Alkanes: Single-Crystal X-Ray Analyses of Propane at 30 K and of *n*-Butane to *n*-Nonane at 90 K. *Angew. Chem., Int. Ed.* **1999**, *38*, 988−992.
(21) Amer, M. S.; Elliott, J. A.; Maguire, J. F.; Windle, A. H. Calculations of the Raman Spectra of C60 Interacting with Water Molecules. *Chem. Phys. Lett.* **2005**, *411*, 395−398.
(22) Fermeglia, M.; Ferrone, M.; Pricl, S. Estimation of the Binding Energy in Random Poly(Butylene terephtalate-co-thiodiethylene terephtalate) Copolyesters/Clay Nanocomposites via Molecular Simulation. *Mol. Simul.* **2004**, *30*, 289−300.
(23) Jirapongphan, S. S.; Warzywoda, J.; Budil, D. E.; Sacco, A., Jr. Simulation of Benzene Adsorption in Zeolite HY Using Supercage-Based Docking. *Microporous Mesoporous Mater.* **2006**, *94*, 358−363.
(24) Sun, H. COMPASS: An ab Initio Force-Field Optimized for Condensed-Phase Applications − Overview with Details on Alkane and Benzene Compounds. *J. Phys. Chem. B* **1998**, *102*, 7338−7364.
(25) Zhao, L.; Liu, L.; Sun, H. Semi-ionic Model for Metal Oxides and Their Interfaces with Organic Molecules. *J. Phys. Chem. C* **2007**, *111*, 10610−10617.
(26) Skouras, E. D.; Burganos, V. N.; Payatakes, A. C. Improved Atomistic Simulation of Diffusion and Sorption in Metal Oxides. *J. Chem. Phys.* **2001**, *114*, 545−552.
(27) Kunnmann, W.; Larese, J. Z. Method for the Generation of Variable Density Metal Vapors which Bypasses the Liquidus Phase. U.S. Patent 6,179,897, 2001.
(28) Mursic, Z.; Lee, M. Y. M.; Johnson, D. E.; Larese, J. Z. A Computer-Controlled Apparatus for Performing High-Resolution Adsorption Isotherms. *Rev. Sci. Instrum.* **1996**, *67*, 1886−1890.
(29) Carruth, G. F.; Kobayashi, R. Vapor Pressure of Normal Paraffins Ethane through n-Decane from Their Triple Points to about 10 mm Mercury. *J. Chem. Eng. Data* **1973**, *18*, 115−126.
(30) Linstrom, P. J.; Mallard, W. G. *NIST Chemistry WebBook*; NIST Standard Reference Database Number 69; National Institute of Standards and Technology: Gaithersburg, MD, 2005; http://webbook.nist.gov (accessed February 23, 2013).
(31) Mayer,V.; Svodova, V.International Union of Pure and Applied Chemistry. Enthalpies of vaporization of organic compounds: a critical review and data compilation; IUPAC chemical data series. Blackwell Scientific Publications: Oxford, U.K., 1985; p 300.
(32) Dash, J. G. *Films on Solid Surfaces*; Academic Press: New York, 1974.
(33) Phillips, J. M.; Larese, J. Z. Microscopic Structure and Transitions in Xenon Multilayer Films. *Phys. Rev. B* **1997**, *56*, 15938−15946.
(34) Bixon, M.; Lifson, S. Potential Functions and Conformations in Cycloalkanes. *Tetrahedron* **1967**, *23*, 769−784.
(35) Brooks, B. R.; Bruccoleri, R. E.; Olafson, B. D.; States, D. J.; Swaminathan, S.; Karplus, M. CHARMM: A Program for Macromolecular Energy, Minimization, and Dynamics Calculations. *J. Comput. Chem.* **1983**, *4*, 187−217.
(36) Dennis, J. E., Jr.; Moré, J. J. Quasi-Newton Methods, Motivation and Theory. *SIAM Rev.* **1977**, *19*, 46−89.
(37) Ewald, P. P. The Calculation of Optical and Electrostatic Grid Potential. *Ann. Phys.* **1921**, *64*, 253−287.